in the course of obtaining CFGF expressions, the approximating functions represent spherical waves with complex distances. Hence, types of waves that are different in nature than spherical waves, such as surface waves are not represented properly. Consequently, the proposed CFGF representations are less accurate when the field point is electrically far away from the source location where surface waves start to dominate.

REFERENCES

[1] L. Josefsson and P. Persson, *Conformal Array Antenna Theory and Design*. Piscataway/Hoboken, NJ: IEEE Press/Wiley, 2006.

[2] P. Persson and R. G. Rojas, "High-frequency approximation for mutual coupling calculations between apertures on a perfect electric conductor circular cylinder covered with a dielectric layer: Nonparaxial region," *Radio Sci.*, vol. 38, no. 4, Jul./Aug. 2003.

[3] Y. L. Chow, J. J. Yang, D. F. Fang, and G. E. Howard, "A closed-form spatial Green's function for the thick microstrip substrate," *IEEE Trans. Microwave Theory Tech.*, vol. 39, pp. 588–592, Mar. 1991.

[4] G. Dural and M. I. Aksun, "Closed-form Green's functions for general sources and stratified media," *IEEE Trans. Microwave Theory Tech.*, vol. 43, pp. 1545–1552, Jul. 1995.

[5] M. I. Aksun, "A robust approach for the derivation of closed-form Green's functions," *IEEE Trans. Microwave Theory Tech.*, vol. 44, pp. 651–658, May 1996.

[6] C. Tokgöz, "Derivation of closed-form Green's functions for cylindrically stratified media," M.S. thesis, Dept. Elect. Electron. Eng., Middle East Technical Univ., Ankara, Turkey, 1997.

[7] C. Tokgöz and G. Dural, "Closed-form Green's functions for cylindrically stratified media," *IEEE Trans. Microwave Theory Tech.*, vol. 48, pp. 40–49, Jan. 2000.

[8] J. Sun, C.-F. Wang, L.-W. Li, and M.-S. Leong, "A complete set of spatial-domain dyadic Green's function components for cylindrically stratified media in fast computational form," *J. Electromagn. Waves Appl.*, vol. 16, no. 11, pp. 1491–1509, 2002.

[9] R. C. Acar and G. Dural, "Comments on a complete set of spatial-domain dyadic Green's function components for cylindrically stratified media in fast computational form," *J. Electromagn. Waves Appl.*, vol. 18, no. 10, pp. 1389–1394, 2004.

[10] J. Sun, C.-F. Wang, L.-W. Li, and M.-S. Leong, "Reply to comments on a complete set of spatial-domain dyadic Green's function components for cylindrically stratified media in fast computational form," *J. Electromagn. Waves Appl.*, vol. 18, no. 10, pp. 1395–1398, 2004.

[11] J. Sun, C.-F. Wang, L.-W. Li, and M.-S. Leong, "Further improvement for fast computation of mixed potential Green's functions for cylindrically stratified media," *IEEE Trans. Antennas Propag.*, vol. 52, pp. 3026–3036, Nov. 2004.

[12] S. Karan, V. B. Erturk, and A. Altintas, "Closed-form Green's function representations in cylindrically stratified media for method of moments applications," *IEEE Trans. Antennas Propag.*, vol. 57, pp. 1158–1168, Apr. 2009.

[13] C. A. Balanis, *Advanced Engineering Electromagnetics*. New York: Wiley, 1989.

[14] Y. Hua and T. K. Sarkar, "Generalized pencil-of-function method for extracting poles of an EM system from its transient response," *IEEE Trans. Antennas Propag.*, vol. 37, pp. 229–234, Feb. 1989.

[15] M. Abramowitz and I. A. Stegun, *Handbook of Mathematical Functions With Formulas, Graphs, and Mathematical Tables*. Mineola, NY: Dover, 1970.

[16] CST MWS, SP1 [DVD-ROM]. Darmstadt, Germany, 2011.

Multiwall Carbon Nanotubes at RF-THz Frequencies: Scattering, Shielding, Effective Conductivity, and Power Dissipation

Jay A. Berres and George W. Hanson

***Abstract*—Isolated, infinitely long multiwall carbon nanotubes (MWCNTs) interacting with electromagnetic waves in the microwave and far-infrared frequency regime are analyzed using a semi-classical approach. An expression for the bulk effective conductivity of MWCNTs is obtained, valid up to THz frequencies. The influence of the number of tube walls, the radius of the outermost tube wall, and the presence of a gold core on scattering and shielding is analyzed. Comparisons between metallic MWCNTs, metallic single wall carbon nanotubes (SWCNTs), and metal nanowires are provided.**

***Index Terms*—Carbon nanotube, electromagnetic theory, nanotechnology.**

I. INTRODUCTION

Carbon nanotubes (CNTs) continue to be at the forefront of research today, since their physical properties make them promising candidates for nanoscale applications. They can form naturally into two types, single wall carbon nanotubes (SWCNTs) and multiwall carbon nanotubes (MWCNTs). A MWCNT consists of multiple co-centric SWCNTs, where the distance between each tube wall is approximately 0.34 nm, which is the distance between interatomic layers of graphite (i.e., graphene sheets) [1]. The number of tube walls for a MWCNT can vary anywhere from 2 to several hundred. Typically the length of CNTs can be from the nanometer scale up to centimeters, and in the case of SWCNTs, their cross-sectional radius varies within the range of approximately 0.3 to 2–5 nm. For MWCNTs, their overall cross-sectional radius varies within the range of approximately 1 to 100 nm. The electromagnetic response of CNTs, and their corresponding applications as antennas, interconnects, and thermal contrast agents, are being investigated [2]–[15]. Of the papers that analyze the electromagnetic response of CNTs, the majority of these papers focus on SWCNTs, although [8] and [12] consider MWCNTs, [9] and [11] consider nanotube bundles, and [13] and [14] consider nanotube sheets. From the emerging literature it is becoming clear that for far-infrared applications, individual SWCNTs have losses that are too large (associated with their extremely small radius) to serve as antennas or interconnects. However, bundles of SWCNTs, and individual or bundles of MWCNTs, may be good candidates for antenna and interconnect applications. Furthermore, planar sheets of nanotubes fabricated as conformal patch antennas have shown excellent properties [13], [14].

In this work, the electromagnetic response of an isolated, infinitely long MWCNT is analyzed in the microwave and far-infrared frequency regime using a semi-classical approach. The influence of the number of tube walls, the radius of the outermost tube wall, and the presence of a gold core on scattering and shielding characteristics is analyzed. Comparisons between metallic MWCNTs, metallic SWCNTs, and metal

Manuscript received May 17, 2010; revised November 18, 2010; accepted January 15, 2011. Date of publication June 09, 2011; date of current version August 03, 2011.

The authors are with the Department of Electrical Engineering, University of Wisconsin-Milwaukee, Milwaukee, WI 53211 USA (e-mail: jaberres@gmail.com; george@uwm.edu).

Digital Object Identifier 10.1109/TAP.2011.2158951

nanowires are discussed, and an effective conductivity model is developed for MWCNTs.

The frequency range considered is 10 MHz to 10 THz. The CNTs are infinitely long, which, in practice, means electrically-long. Since the longest CNTs so far produced are in the centimeter range, an $L = 1\ \mathrm{cm}$ CNT can be considered to be electrically-long (say, $L \geq 10\lambda_0$) starting at 300 GHz. If one considers that $\lambda_{tube} \backsimeq \lambda_0/50$ for small radius tubes [4], [5], then an $L = 1\ \mathrm{cm}$ CNT can be considered to be electrically-long ($L \geq 10\lambda_{tube}$) starting at 6 GHz. However, often $L \sim 500\ \mathrm{nm}$ to $L \sim 100\ \mu\mathrm{m}$ long tubes are of interest, which in many cases will not be electrically-long at the frequencies considered in this work. Nevertheless, the analysis of infinite-length tubes provides insight into their intrinsic properties, without the complication of end effects. An example is the utility of the effective conductivity model presented below, which allows a direct comparison of the conductivity of metal nanowires and CNTs in units of S/m. Importantly, when a CNT bridges two electrodes, current does not become zero at the tube ends. In this case, end effects are diminished even for electrically-short tubes, and the infinite-length tube properties (say, attenuation per unit length) are of interest. As an example, in [16] a massively parallel array of electrically-short CNTs bridging two electrodes showed that they combined essentially in parallel, which does not occur when end effects are important.

Given the geometry of MWCNTs, the potential for inter-tube-wall electron tunneling exists. Based on the analysis in [12], this tunneling can be ignored if there is minimal difference in the total field from tube wall to tube wall. From Fig. 3 it can be seen that this requirement is satisfied. Therefore, inter-tube-wall electron tunneling can be ignored in the model developed here. In the following, the time variation (suppressed) is $e^{j\omega t}$, and TM^z polarization is considered since this results in the largest component of the induced current density.

II. Theory and Formulation

A SWCNT can be envisioned as a rolled-up graphene sheet (i.e., a monoatomic layer of graphite), and is characterized by the dual index (m, n), where $(m, 0)$ results in zigzag CNTs, (m, m) results in armchair CNTs, and (m, n), $0 < n \neq m$, results in chiral CNTs. The resulting cross-sectional radius of a SWCNT is [1], $a = |\mathbf{C}_h|/2\pi = \left(\sqrt{3}b\sqrt{m^2 + mn + n^2}\right)/2\pi$, where $b = 0.142\ \mathrm{nm}$ is the interatomic distance between carbon atoms in graphene. Armchair CNTs are always metallic (they exhibit no energy bandgap) as are zigzag CNTs with $m = 3q$, where q is an integer (although zigzag tubes can have a small bandgap due to curvature effects, one can usually consider them as metallic from an applications perspective). With $m \neq 3q$, zigzag CNTs are semiconducting. MWCNTs can be envisioned as multiple co-centric SWCNTs, and can be an ensemble of all metallic SWCNTs, all semiconducting SWCNTs, or a combination of both. However, for $a \geq 10\ \mathrm{nm}$ or so additional electron channels make the tube walls tend towards the graphene value, independent of m, n.

Assuming a spatially local response, the considered frequency range is below the onset of optical interband transitions even for large-radius tubes (e.g., for metallic tubes the onset of interband transitions occurs at approximately [2] $hf = 3\gamma_o b/2a$, where γ_o is given below). Thus, we can ignore the interband contribution to conductivity. The semiclassical intraband conductivity (S) is given by [2], [17]

$$\sigma = \sigma_{cn} = \frac{je^2}{\pi^2\hbar a}\frac{1}{(\omega - j\nu)}\sum_{s=1}^{m}\int_{1stBZ}\frac{\partial F_c}{\partial p_z}\frac{\partial \varepsilon_c}{\partial p_z}dp_z, \qquad (1)$$

where e is the charge of an electron, $\nu = \tau^{-1}$ is the phenomenological relaxation frequency (τ being the relaxation time), $\hbar$ is the reduced Planck's constant, and F_c is the equilibrium Fermi distribution function. The conductivity for an armchair or zigzag CNT can then be determined by specifying ε_c, the electron dispersion relation, performing the summation over the quantized quasimomentum states, and integrating over the first Brillouin zone [2].

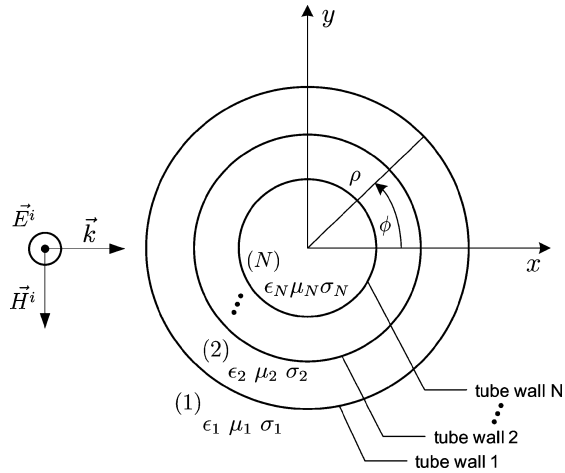

Fig. 1. General model for structures of interest (infinitely long MWCNT, SWCNT, or material cylinder) with incident TM^z wave.

In the following we use $\nu = \tau^{-1} = 12T/2a$ [18], where T is the temperature in Kelvin. The appropriate value of relaxation frequency ν for a MWCNT is difficult to determine (among other complicating factors, there should be a relaxation frequency for each shell, but measurement will determine one (collective) mean-free path (MFP) and equivalent relaxation frequency for a given MWCNT). Some MWCNTs are highly disordered and contain many defects, and for those MFPs on the order of 10 nm or less are appropriate. However, several measurements on ordered coaxial MWCNTs, which are under investigation here, have shown very long MFPs, as large as 25–30 $\mu\mathrm{m}$ [19]. Using the relaxation frequency as specified above, we do indeed obtain MFPs up to several tens of micrometers for large-radius shells.

A. MWCNT, SWCNT, and Material Cylinder

Consider an infinitely long circular cross-sectional multiregion cylinder oriented along the z axis, as shown in Fig. 1. A uniform plane wave is normally incident on the structure, $\mathbf{E}^i = \hat{\mathbf{z}}E_z^i = \hat{\mathbf{z}}E_0 e^{-jkx}$.

The boundary conditions at each tube wall are [2] $E_z^{(+)} = E_z^{(-)} = E_z$, $H_\phi^{(+)} - H_\phi^{(-)} = J_s = \sigma E_z$, where $(+)$ and $(-)$ correspond to the region on the outside and inside of the tube wall, respectively, and σ corresponds to the surface conductivity of the particular tube wall (each wall can have a different conductivity). Following the usual procedure for scattering from cylinders, we can write the total field in the exterior region (1) as $E_z^{(1)} = E_0\sum_{n=-\infty}^{\infty} j^{-n}(J_n(k_1\rho) + a_{n1}H_n^{(2)}(k_1\rho))e^{jn\phi}$, the total field in the innermost region (N) as $E_z^{(N)} = E_0\sum_{n=-\infty}^{\infty} j^{-n}a_{nN}J_n(k_N\rho)e^{jn\phi}$, and the total field in each interwall region (m), where $1 < m < N$, as $E_z^{(m)} = E_0\sum_{n=-\infty}^{\infty} j^{-n}(a_{nm}J_n(k_m\rho) + b_{nm}Y_n(k_m\rho))e^{jn\phi}$. The relevant magnetic field components can be easily obtained from Maxwell's equations. Using the field expansions, the boundary conditions lead to a system of equations that can be solved for the unknown coefficients. As a special case, for a SWCNT of radius a having $k_1 = k_2$ [7], $a_{n1} = -\eta\sigma(J_n(ka))^2/D$ and $a_{n2} = 2/\pi ka/D$, where $D = 2/\pi ka + \eta\sigma H_n^{(2)}(ka)J_n(ka)$.

We also want to consider the case of a material cylinder, to compare the CNT to metal nanowires. We can simply use the above formulation and set the surface conductivity to

zero. For the special case of a homogeneous cylinder, $a_{n1} = (J_n'(k_1a)J_n(k_2a) - \eta_1/\eta_2 J_n'(k_2a)J_n(k_1a))/D_m$, $a_{n2} = \left(J_n'(k_1a)H_n^{(2)}(k_1a) - J_n(k_1a)H_n^{(2)\prime}(k_1a)\right)/D_m$, where $D_m = \eta_1/\eta_2 J_n'(k_2a)H_n^{(2)}(k_1a) - J_n(k_2a)H_n^{(2)\prime}(k_1a)$, $\eta = \sqrt{\mu/\epsilon_c}$, and where the prime denotes differentiation with respect to the argument. A perfect electric conductor (PEC) cylinder can be recovered by letting the conductivity of the region become infinite, resulting in $a_{n1} = -J_n(ka)/H_n^{(2)}(ka)$.

B. Effective Conductivity of MWCNTs

It is often stated that SWCNTs are better conductors than metals, but the meaning of this statement is somewhat unclear since it is impossible to directly compare the conductivity of a metal (S/m) with the surface conductivity of a CNT tube wall (S). In order to facilitate this comparison, in this section we determine an effective bulk conductivity for the CNT based on complex power flow, which allows the MWCNT to be treated as an effectively solid material cylinder (when the specific geometry of the cylinder, solid or hollow, is unimportant).

An effective conductivity can be obtained by equating the power dissipated in a material cylinder to that of a MWCNT of equal outer radius. This can be accomplished analytically provided that the Born approximation is applicable, which means that the total field internal to the structure is approximately equal to the incident field. Based on the results in Section III-A, we find that the Born approximation is applicable up to THz frequencies (this does not hold for finite-length, electrically-short MWCNTs, which aren't considered here).

The power dissipated (per unit length) in an infinite-length material cylinder is

$$P_{mat} = \frac{1}{2} Re\left(\sigma_{mat}^*\right) \int_S |\mathbf{E}|^2 d^2r \tag{2}$$

W/m, where σ_{mat}^* is the complex-valued bulk conductivity of the material, and $\mathbf{E}$ is the electric field in the cylinder. Since, $ka \ll 1$, only the $n = 0$ term is important and a_{n2} reduces to [15] $a_{02} = c_0 \simeq 1/\left(1 - \pi k_2 a^2/4j\,(1 - j2/\pi \ln(k_1 a/2))\right)$, such that (2) becomes

$$P_{mat} = \frac{\pi}{2} a^2 Re\left(\sigma_{mat}^*\right) E_0^2 |c_0|^2. \tag{3}$$

Similarly, the power dissipated in a SWCNT is

$$P_{swcnt} = \frac{1}{2} Re\left(\sigma_{cnt}^*\right) \int_0^{2\pi} |\mathbf{E}|^2 a d\phi \tag{4}$$

W/m, where σ_{cnt}^* is the complex-valued conductivity of the CNT and $\mathbf{E}$ is the electric field at the wall of the CNT. Since $ka \ll 1$, keeping only the $n = 0$ term and calling $a_{n1} = a_0$,

$$P_{swcnt} = \pi a Re\left(\sigma_{cnt}^*\right) E_0^2 |A_0|^2, \tag{5}$$

where, $A_0 = 1 + a_0 H_0^{(2)}(ka)$. Again, assuming $ka \ll 1$, it can be shown that $c_0 \to 1$ and $A_0 \to 1$ using $\lim_{x\to 0}(x \ln(x)) = 0$. Note that the approximation $c_0 = A_0 = 1$ is exactly the Born approximation. Then, (3) becomes

$$P_{mat} = \frac{\pi}{2} a^2 Re\left(\sigma_{mat}^*\right) E_0^2, \tag{6}$$

and (5) becomes

$$P_{swcnt} = \pi a Re\left(\sigma_{cnt}^*\right) E_0^2. \tag{7}$$

From [12], the power dissipated in a MWCNT, under the Born approximation, leads to

$$P_{mwcnt} = \frac{1}{2} Re\left(\sum_{tw=1}^{N} 2\pi a_{tw} \sigma_{cnt,tw}^*\right) E_0^2. \tag{8}$$

W/m, where a_{tw} is the radius of the relevant tube wall, $\sigma_{cnt,tw}^*$ is the complex-valued conductivity at the relevant tube wall, and N is the number of tube walls.

The effective conductivity for a SWCNT is obtained by equating complex power for a SWCNT and for a material cylinder (these are (6) and (7) with the real-part operator removed), which, upon re-naming σ_{mat}^* as σ_{mat}^{eff*}, becomes

$$\sigma_{mat}^{eff*} = \frac{2}{a} \sigma_{cnt}^*. \tag{9}$$

Similarly, the effective conductivity for a MWCNT is obtained by equating complex power for a MWCNT and for a material cylinder (these are (6) and (8) without the real-part operator), leading to

$$\sigma_{mat}^{eff*} = \frac{2}{a^2} \sum_{tw=1}^{N} a_{tw} \sigma_{cnt,tw}^*, \tag{10}$$

where a is the radius of the outermost tube wall. Note that for $N = 1$, (i.e., a SWCNT), (10) becomes (9).

In order to check the validity of the effective conductivity expression, the exact power dissipated for MWCNTs, calculated directly from the multiwall scattering formulation without the Born approximation, was compared to the power dissipated using the conductivity σ_{mat}^{eff*} in place of σ_{mat}^* in (2). The two methods show excellent agreement. As an additional check, numerical values for the fields (evaluated at the origin of the cylinder, and at a quarter of a wavelength away from the cylinder) of a MWCNT were compared to those arising from the analytical expressions for a material cylinder having effective conductivity σ_{mat}^{eff*}. Again, excellent agreement was found.

III. Results

Given the small radius of CNTs ($ka \ll 1$), rapid convergence of the field expressions was obtained (often only the $n = 0$ term was needed). For the CNTs, all regions inside, outside and between tube walls are free space. In order to keep the distance between tube walls to be approximately 0.34 nm, in most of the following results we will consider MWCNTs consisting of armchair (metallic) walls with an increase in the index $m = n$ of 5, which preserves the required inter-wall spacing. The validity of the tube wall conductivity and scattering model for the single wall case has been discussed in [20]. It was found that the tube wall conductivity (1) leads to good agreement with measurement for tube resistance and kinetic inductance. No measured scattering results are available for individual MWCNTs, although the result in [21] gives confidence in the MWCNT model in the far-infrared frequency regime.

A. Electromagnetic Scattering and Shielding

Fig. 2 shows scattering results for a 3 wall and a 10 wall MWCNT, where in both cases the innermost tube is (10,10). The strong frequency dependence of the scattered field is evident, due to the strong frequency dependence of the conductivity (right axis). Additionally, the scattered field is greater for the 10 wall MWCNT when compared to that of the 3 wall MWCNT, indicating the additional contribution to the scattered field from the larger structure and number of walls.

Given that additional tube walls seem to play an important role in enhancing scattering, the amount of electromagnetic shielding provided by tube walls was investigated. One might reasonably expect the outer tube walls in a MWCNT to shield the inner tube walls from the incident field. However, this turns out not to be the case for infinitely long MWCNTs at moderately low frequencies (for finite-length, electrically-short MWCNTs the situation is different). Fig. 3 shows the magnitude of the total electric field inside a 50 wall MWCNT having innermost wall (5,5) (radius is 0.339 nm) and outermost wall (250,250) (radius is 16.95 nm), as a function of position within the structure. It can be seen that, in general, individual tube walls provide little shielding,

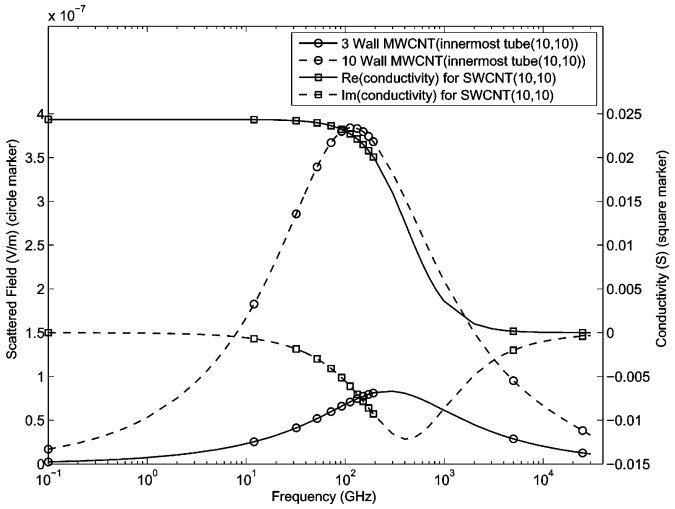

Fig. 2. Magnitude of scattered field (left side axis) for a 3 wall MWCNT and 10 wall MWCNT, both having innermost tube being (10,10), and conductivity (right side axis) for a (10, 10) tube wall at frequencies in the microwave and far-infrared frequency bands. The field is evaluated in the far field at $\rho_{ff} = 0.477$ km.

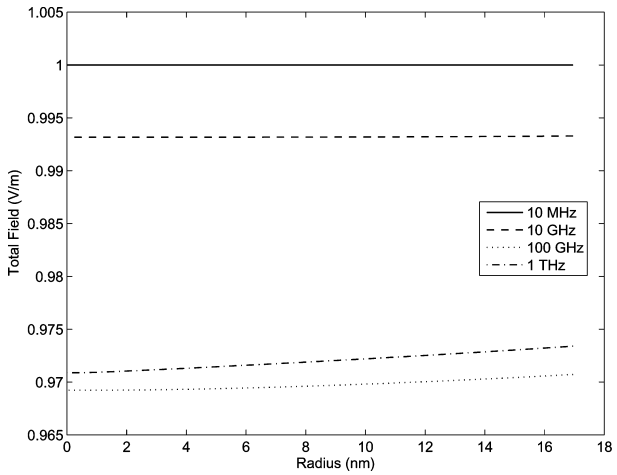

Fig. 3. Magnitude of total electric field inside a 50 wall MWCNT (innermost tube is (5,5), having a radius of 0.339 nm, and the outermost tube is (250,250), having a radius of 16.95 nm) as a function of position at 10 MHz, 10 GHz, 100 GHz, and 1 THz frequencies.

with shielding essentially non-existent at the lower frequencies. Although not shown, it turns out that one would require a hypothetical surface conductivity of $\sigma = 10^5$ S for the wall of a 1.7 nm radius tube to shield the inside region from the incident field at 10 MHz, and $\sigma \sim 10^3$ S at 10 GHz. Obviously, these are nonphysical values.

B. MWCNT, SWCNT, and Metal Nanowire Comparison

In this section, a comparison between metallic MWCNTs, metallic SWCNTs, and metal nanowires is provided. For the metal nanowire, the conductivity must account for the frequency dependence of the bulk metal, as well as the size-dependent effects due to the nanoscale wire radius having dimensions on the order of or less than the electronic mean free path. Here we use the bulk conductivity in the far-infrared and microwave regimes given by the Drude form, and account for size-dependent effects as in [6].

In a MWCNT, scattering is affected by the number of tube walls, the radius of the inner wall, and the radius of the outer wall. It is not clear, a priori, how these factors interrelate, and which factors are the most important in scattering. For example, is the scattered field larger for a large-radius, few wall MWCNT, or for a smaller-radius, many wall MWCNT? In order to answer this question, Fig. 4 shows a composite plot (ten different MWCNT geometries) of the radar cross section (RCS)

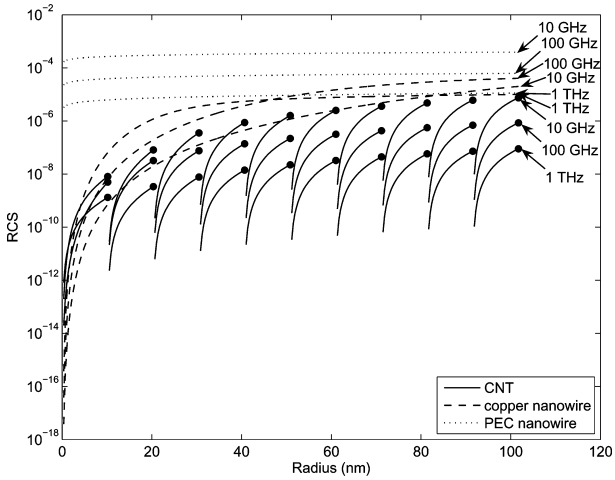

Fig. 4. RCS for ten different MWCNT geometries (each up to 30 wall), copper nanowire, and PEC nanowire versus radius at 10 GHz, 100 GHz, and 1 THz frequencies. This is a composite plot for ten different CNT sets, as explained in the text.

$$RCS_{2D} = RCS = \lim_{\rho \to \infty} 2\pi\rho \frac{|\mathbf{E}^s|^2}{|\mathbf{E}^i|^2} \tag{11}$$

versus radius, at several different frequencies (10 GHz, 100 GHz, and 1 THz frequencies). For comparison, results for a copper nanowire and for a PEC nanowire are also shown. For the copper and PEC nanowires, radius was simply increased over the indicated range. For the MWCNT (referred to in the legend as CNT), results were obtained in the following manner. The first data point was for a (5,5) SWCNT. The second was for a 2 wall MWCNT having innermost tube (5,5) and outermost tube (10,10). We repeated this scenario, i.e., adding outer tube walls, increasing the index m by 5 each time, until we reached a 30 wall MWCNT, where the outermost tube will be (150,150), having radius 10.17 nm. That first section is clear on the left side of the plot, and constitutes the first MWCNT geometry. For the second MWCNT geometry, we started over with a (155,155) SWCNT (radius 10.51 nm), then added as an outer wall a (160,160) tube, and kept adding outer walls until we again reached a 30 wall MWCNT, in which case the outermost wall will be (300,300), having radius 20.34 nm. This second MWCNT case is evident as the second (from the left) section of the figure. This was continued until we reached the tenth MWCNT geometry (evident as the right-most section on the plot), where we started with a (1355,1355) SWCNT (radius is 91.87 nm) and added outer walls until we reached a 30 wall MWCNT having outer wall (1500,1500) (radius is 101.7 nm).

From this figure we can draw several conclusions. First, a realistic model for metal nanowires is important at these radii values, since the scattered fields from a metal nanowire are much smaller than for a PEC nanowire. Second, for very small radii, on the order of a few nanometers, electromagnetic scattering is greater for SWCNTs and MWCNTs than it is for copper nanowires, whereas the opposite is the case for larger radii. This is explained in terms of effective conductivity in the subsequent results. Third, scattering in a MWCNT increases as tube walls are added. For each geometry in this figure, we start with a SWCNT and add exterior tube walls, increasing the outer radius of the structure. However, we also found that starting with a SWCNT and adding interior tube walls, so that the outer radius

of the structure is unchanged, also increases the scattered field in a similar manner. Fourth, by comparing the equivalent data points in each section (e.g., the final data points in each section, representing 30 wall MWCNTs, are indicated by dots), a larger N wall MWCNT will scatter more strongly than a smaller N wall MWCNT. This trend seems to level off for the largest radius values considered, especially at 100 GHz and 1 THz. For example, comparing the two right-most sections of the plot, the ninth 30 wall MWCNT geometry (outer radius 91.53 nm) scatters approximately the same field as the tenth 30 wall MWCNT geometry (outer radius 101.7 nm). This is clearly not the case for the first several 30 wall MWCNT geometries, especially at the two lower frequencies.

C. MWCNT With a Gold Core

The electromagnetic response of a MWCNT with a gold core is investigated. It is beneficial to look at the response of such a structure to see what role the tube walls play in the overall response. Applications include coaxial-like transmission lines, and in using a SWCNT or MWCNT to act as a template to facilitate the growth of gold wires [12].

From our investigation we found that for the smaller outermost tube wall radii, the electromagnetic response of the structure is commensurate with the electromagnetic response of the MWCNT itself. That is, the presence or absence of a gold core makes no difference in the scattering from the structure. This is explained by the relatively large effective conductivity of a small radius MWCNT (described in Section IV), which is, effectively, a better conductor than the gold core. For the larger radii case the scattered field is essentially that of the gold core, since the effective conductivity of a large radius, small number of wall MWCNT is much lower than that of gold.

D. Effective Conductivity and Power Dissipation

The effective conductivity (10) for various MWCNTs is shown in Table I at $f = 10\ \mathrm{MHz}$, chosen due to the RF heating applications in [22]. Also shown is the effective conductivity normalized by the value of the bulk conductivity of gold $\left(\sigma_{au}^{*} = 4.9 \times 10^{7} - j9.074 \times 10^{1}\ \mathrm{S/m}\right)$, and the power dissipated in the tube by an incident, unit amplitude plane wave.

From Table I, it can be observed that all of the CNT geometries considered have an effective conductivity better than bulk gold (by nearly a factor of three for the SWCNT). Comparing with a metal nanowire and considering the radius-dependent effect, one may see that the SWCNT and small-radius MWCNTs are better conductors than a gold nanowire. Furthermore, CNTs can often be grown with few defects, whereas small radius nanowires often have many defects and would actually have much higher losses than assumed here. In fact, it is unlikely that a gold nanowire can be fabricated with radius much less than 5 nm, and so the comparison for the smallest radius values is somewhat artificial.

Regarding power dissipation for possible heating applications, for infinitely long, fixed-radius cylinders, power dissipation increases as conductivity increases (this is not the case for electrically-short cylinders [15]). From Table I, although effective conductivity generally falls as radius is increased, power dissipation increases due to the geometric dependence on cross-sectional area (see, e.g., (6)).

The effective conductivity and power dissipated for semiconducting tubes are shown in Table II, where the semiconducting tubes are zigzag CNTs (innermost tube (8,0)), and the m index for each additional tube wall increased by a factor of 9. Obviously the effective conductivity of small-radius MWCNTs constructed from semiconducting tubes is much smaller than for gold. However, larger-radius MWCNTs made from semiconducting walls have values of effective conductivity and power dissipation comparable to similarly-sized MWCNTs made from metallic walls. As described previously, for tube radius more than approximately 10 nm the value of surface conductivity approaches that of graphene, and becomes independent of tube indices (m, n). The large difference between the single wall and double wall cases arises from the strong difference in shell conductivity of the first two shells; succeeding shells differ in conductivity to a lesser extent.

TABLE I
EFFECTIVE CONDUCTIVITY AND POWER DISSIPATION VALUES FOR METALLIC CNTS (INNERMOST TUBE (5,5)) AT 10 MHz

CNT (innermost tube (5,5))	Outermost tube wall radius (nm)	Effective conductivity σ_{mat}^{eff*} (S/m)	$\sigma_{\mathrm{mat}}^{\mathrm{eff}*}/\sigma_{\mathrm{au}}^{*}$	Power dissipated (W/m)
SWCNT	0.339	$1.436\times10^{8} - j1.729\times10^{3}$	$2.931 - j2.986\times10^{-5}$	2.593×10^{-11}
2 wall MWCNT	0.678	$1.077\times10^{8} - j2.161\times10^{3}$	$2.198 - j4.003\times10^{-5}$	7.779×10^{-11}
3 wall MWCNT	1.017	$9.576\times10^{7} - j2.689\times10^{3}$	$1.954 - j5.126\times10^{-5}$	1.556×10^{-10}
4 wall MWCNT	1.356	$8.978\times10^{7} - j3.241\times10^{3}$	$1.832 - j6.275\times10^{-5}$	2.593×10^{-10}
5 wall MWCNT	1.695	$8.619\times10^{7} - j3.803\times10^{3}$	$1.759 - j7.435\times10^{-5}$	3.890×10^{-10}
10 wall MWCNT	3.390	$7.905\times10^{7} - j6.661\times10^{3}$	$1.613 - j1.330\times10^{-4}$	1.427×10^{-9}
15 wall MWCNT	5.085	$7.717\times10^{7} - j9.619\times10^{3}$	$1.575 - j1.934\times10^{-4}$	3.134×10^{-9}
20 wall MWCNT	6.780	$7.747\times10^{7} - j1.284\times10^{4}$	$1.581 - j2.591\times10^{-4}$	5.594×10^{-9}

TABLE II
EFFECTIVE CONDUCTIVITY AND POWER DISSIPATION VALUES FOR SEMICONDUCTING CNTS (INNERMOST TUBE (8,0)) AT 10 MHz

CNT (innermost tube (8,0))	Outermost tube wall radius (nm)	Effective conductivity σ_{mat}^{eff*} (S/m)	$\sigma_{\mathrm{mat}}^{\mathrm{eff}*}/\sigma_{\mathrm{au}}^{*}$	Power dissipated (W/m)
SWCNT	0.313	$9.716\times10^{-4} + j1.523\times10^{-2}$	$1.983\times10^{-11} + j3.108\times10^{-10}$	3.693×10^{-20}
2 wall MWCNT	0.665	$4.593\times10^{2} + j7.930\times10^{-3}$	$9.373\times10^{-6} + j1.792\times10^{-10}$	3.195×10^{-16}
3 wall MWCNT	1.018	$2.090\times10^{4} - j7.290\times10^{-1}$	$4.265\times10^{-4} - j1.409\times10^{-8}$	3.400×10^{-14}
4 wall MWCNT	1.370	$1.333\times10^{5} - j6.311$	$2.720\times10^{-3} - j1.238\times10^{-7}$	3.932×10^{-13}
5 wall MWCNT	1.722	$4.172\times10^{5} - j2.433\times10^{1}$	$8.514\times10^{-3} - j4.808\times10^{-7}$	1.944×10^{-12}
10 wall MWCNT	3.484	$4.951\times10^{6} - j5.390\times10^{2}$	$0.101 - j1.081\times10^{-5}$	9.438×10^{-11}
15 wall MWCNT	5.245	$1.275\times10^{7} - j2.001\times10^{3}$	$0.260 - j4.035\times10^{-5}$	5.510×10^{-10}
20 wall MWCNT	7.007	$2.159\times10^{7} - j4.403\times10^{3}$	$0.441 - j8.904\times10^{-5}$	1.665×10^{-9}

IV. CONCLUSIONS

The electromagnetic response of isolated, infinitely long multiwall carbon nanotubes interacting with electromagnetic plane waves was an-

alyzed. It was found for MWCNTs, there was little shielding due to the presence of multiple tube walls. It was determined that electromagnetic scattering increases as the number of tube walls increase, and as the outermost tube wall radius increases. In general, electromagnetic scattering is greater for metallic MWCNTs than it is for metallic SWCNTs. An equation for the effective conductivity of a MWCNT was presented, and comparisons with metal nanowires were made. For metallic tube walls, effective conductivity decreases slightly as MWCNT size increases, although for semiconducting walls effective conductivity increases dramatically as size increases. In both cases, power dissipation increases with increasing size due to both electrical and geometric effects.

REFERENCES

[1] R. Saito, G. Dresselhaus, and M. S. Dresselhaus, *Physical Properties of Carbon Nanotubes*. U.K.: Imperial College Press, 2003.

[2] G. Y. Slepyan, S. A. Maksimenko, A. Lakhtakia, O. Yevtushenko, and A. V. Gusakov, "Electrodynamics of carbon nanotubes: Dynamic conductivity, impedance boundary conditions, and surface wave propagation," *Phys. Rev. B*, vol. 60, pp. 17136–17149, 1999.

[3] Y. Wang, K. Kempa, B. Kimball, J. B. Carlson, G. Benham, W. Z. Li, T. Kempa, J. Rybczynski, A. Herczynski, and Z. F. Ren, "Receiving and transmitting light-like radio waves: Antenna effect in arrays of aligned carbon nanotubes," *Appl. Phys. Lett.*, vol. 85, no. 13, pp. 2607–2609, 2004.

[4] P. J. Burke, S. Li, and Z. Yu, "Quantitative theory of nanowire and nanotube antenna performance," *IEEE Trans. Nano.*, vol. 5, no. 4, pp. 314–334, 2006.

[5] G. W. Hanson, "Fundamental transmitting properties of carbon nanotube antennas," *IEEE Trans. Antennas Propag.*, vol. 53, pp. 3426–3435, 2005.

[6] G. Hanson, "Radiation efficiency of nanoradius dipole antennas in the microwave and far-infrared regime," *IEEE Antennas Propag. Mag.*, vol. 50, pp. 66–77, 2008.

[7] S. M. Mikki and A. A. Kishk, "Theory of optical scattering by carbon nanotubes," *Microw. Opt. Tech. Letts.*, vol. 49, pp. 2360–2364, 2007.

[8] S. Mikki and A. Kishk, "Electromagnetic scattering by multi-wall carbon nanotubes," *Progr. Electromagn. Res. B*, vol. 17, pp. 49–67, 2009.

[9] M. V. Shuba, S. A. Maksimenko, and A. Lakhtakia, "Electromagnetic wave propagation in an almost circular bundle of closely packed metallic carbon nanotubes," *Phys. Rev. B*, vol. 76, no. 15, pp. 155407–155407, Oct. 2007.

[10] G. Y. Slepyan, M. V. Shuba, S. A. Maksimenko, and A. Lakhtakia, "Theory of optical scattering by achiral carbon nanotubes and their potential as optical nanoantennas," *Phys. Rev. B*, vol. 73, no. 19, pp. 195416–195416, May 2006.

[11] Y. Huang, W.-Y. Yin, and Q. H. Liu, "Performance prediction of carbon nanotube bundle dipole antennas," *IEEE Trans. Nano.*, vol. 7, no. 3, pp. 331–337, 2008.

[12] M. V. Shuba, G. Y. Slepyan, S. A. Maksimenko, C. Thomsen, and A. Lakhtakia, "Theory of multiwall carbon nanotubes as waveguides and antennas in the infrared and the visible regimes," *Phys. Rev. B*, vol. 79, no. 15, pp. 155403–155403, 2009.

[13] T. A. Elwi, H. M. Al-Rizzo, D. G. Rucker, E. Dervishi, Z. Li, and A. S. Biris, "Multi-walled carbon nanotube-based rf antennas," *Nanotechnology*, vol. 21, no. 4, pp. 045301–045301, 2010.

[14] Y. Zhou, Y. Bayram, F. Du, L. Dai, and J. L. Volakis, "Polymer-carbon nanotube sheets for conformal load bearing antennas," *IEEE Trans. Antennas Propag.*, vol. 58, no. 99, pp. 2169–2175, Jul. 2010.

[15] G. W. Hanson and S. K. Patch, "Optimum electromagnetic heating of nanoparticle thermal contrast agents at rf frequencies," *J. Appl. Phys.*, vol. 106, pp. 054309–054309, 2009.

[16] C. Rutherglen, D. Jain, and P. Burke, "Rf resistance and inductance of massively parallel single walled carbon nanotubes: Direct, broadband measurements and near perfect 50 ohm impedance matching," *Appl. Phys. Lett.*, vol. 93, pp. 083119–083119, 2008.

[17] S. Maksimenko, G. Slepyan, O. N. Singh, and A. Lakhtakia, *Electromagnetic Fields in Unconventional Materials and Structures*. New York: Wiley, 2000, vol. Electrodynamic Properties of Carbon Nanotubes.

[18] X. Zhou, J.-Y. Park, S. Huang, J. Liu, and P. L. McEuen, "Band structure, photon scattering, and the performance limit of single-walled carbon nanotube transistors," *Phys. Rev. Lett.*, vol. 95, pp. 146805–146805, 2005.

[19] H. J. Li, W. G. Lu, J. J. Li, X. D. Bai, and C. Z. Gu, "Multichannel ballistic transport in multiwall carbon nanotubes," *Phys. Rev. Lett.*, vol. 95, pp. 086601–086601, 2005.

[20] J. Hao and G. W. Hanson, "Infrared and optical properties of carbon nanotube dipole antennas," *IEEE Trans. Nano.*, vol. 5, pp. 766–775, 2006.

[21] G. Y. Slepyan, M. V. Shuba, and S. A. Maksimenko, "Terahertz conductivity peak in composite materials containing carbon nanotubes: Theory and interpretation of experiment," *Phys. Rev. B*, vol. 81, pp. 035020–035020, 2010.

[22] C. J. Gannon, P. Cherukuri, B. I. Yakobson, L. Cognet, J. S. Kanzius, C. Kittrell, R. B. Weisman, M. Pasquali, H. K. Schmidt, R. E. Smalley, and S. A. Curley, "Carbon nanotube-enhanced thermal destruction of cancer cells in a noninvasive radiofrequency field," *Cancer*, vol. 110, no. 12, pp. 2654–2665, Dec. 2007.

Sub-mm Wet Etched Linear to Circular Polarization FSS Based Polarization Converters

M. Euler, V. Fusco, R. Dickie, R. Cahill, and J. Verheggen

***Abstract*—This communication investigates the potential for fabrication of micromachined silicon sub-millimeter wave periodic arrays of freestanding slot frequency selective surfaces (FSS) using wet etch KOH technology. The vehicle for this is an FSS for generating circularly polarized signals from an incident linearly polarized signal at normal incidence to the structure. Principal issues and fabrication processes involved from the initial design of the core FSS structures to be made and tested through to their final testing are addressed. Measured and simulated results for crossed and ring slot element shapes in single and double layer polarization convertor structures are presented for sub-mm wave operation. It is shown that 3 dB axial ratio (AR) bandwidths of 21% can be achieved with the one layer perforated screen design and that the rate of change is lower than the double layer structures. An insertion loss of 1.1 dB can be achieved for the split circular ring double layer periodic array. These results are shown to be compatible with the more specialized fabrication equipment dry reactive ion etching approach previously used for the construction of this type of structure.**

***Index Terms*—Circular-polarization, frequency selective surfaces (FSS), split ring resonator.**

I. INTRODUCTION

Transmission-type polarizers are anisotropic media, which, when placed over a radiating aperture, convert linearly polarized (LP) signals into circularly polarized (CP) signals. [1] Polarization transformers are important in many antenna applications, for instance these can be used to switch the polarization of a satellite's antenna from linear to circular or vice versa. They may also be used in the elimination of rain echoes or for the suppression of interference. A variety of means for achieving a

Manuscript received October 18, 2010; revised November 27, 2010; accepted December 02, 2010. Date of publication June 09, 2011; date of current version August 03, 2011. This work was supported in part by a N Ireland Department for Employment and Learning (DEL) Ph.D. Scholarship and Strengthening all Island grants, the Science Foundation Ireland National Access Programme (Grant NAP-151), and in part by the U.K. Engineering and Physical Science Research Council under Grant EP/E01707/X.

M. Euler, V. Fusco, R. Dickie, and R. Cahill are with The Institute of Electronics, Communications and Information Technology, Queen's University Belfast, Queen's Island, Belfast BT3 9DT, Northern Ireland, U.K. (e-mail: v.fusco@ecit.qub.ac.uk).

J. Verheggen is with the Tyndall National Institute, Dyke Parade, Cork, Ireland.

Digital Object Identifier 10.1109/TAP.2011.2158973